Solid State Ionics 357 (2020) 115456

Contents lists available at ScienceDirect

Solid State Ionics

journal homepage: www.elsevier.com/locate/ssi

Substrate-dependent proton transport and nanostructural orientation of perfluorosulfonic acid polymer thin films on Pt and carbon substrate

Xiao Gao[a], Kentaro Yamamoto[a,*], Tomoyasu Hirai[b], Noboru Ohta[c], Tomoki Uchiyama[a], Toshiki Watanabe[a], Masakuni Takahashi[a], Naoki Takao[d], Hideto Imai[d], Seiho Sugawara[e], Kazuhiko Shinohara[e], Yoshiharu Uchimoto[a]

[a] Graduate School of Human and Environmental Studies, Kyoto University, Yoshida nihonmatsu-cho, Sakyo-ku, Kyoto 606-8501, Japan
[b] Department of Applied Chemistry, Osaka Institute of Technology, 5-16-1 Ohmiya, Asahi-ku, Osaka 535-8585, Japan
[c] Japan Synchrotron Radiation Research Institute (JASRI), Sayo-gun, Hyogo 679-5198, Japan
[d] Nissan Analysis and Research Center, 1, Natsushima-cho, Yokosuka-shi, Kanagawa 237-8523, Japan
[e] Fuel Cell Cutting-Edge Research Center Technology Research Association, 2-3-26, Aomi, Koto-ku, Tokyo 135-0064, Japan

ARTICLE INFO

Keywords:
Nafion thin film
Proton conductivity
Grazing incidence small X-ray scattering

ABSTRACT

The electrochemical reactions occur on the carbon-supported platinum covered by a proton conducting polymer electrolyte. Thus, it is important to clarify the correlation between proton conductivity and morphology of the polymer electrolyte on Pt or carbon. In this study, the properties of thin films (50–200 nm) of Nafion®, which is the typical polymer electrolyte, were investigated on platinum and carbon substrates. Grazing-incidence small/wide angle X-ray scattering and electrochemical impedance spectroscopy were used to extract morphological and proton transport information. Self-designed interdigitated array electrodes were utilized to test and compare the proton conductivity on the Pt and carbon substrates. Based on the results, the difference in anisotropic behavior of Nafion thin films on each substrate were explored, which exhibit that the proton conductivity of Pt-supported Nafion thin films has more well defined hydrophilic domain structure than that of carbon supported thin films along in-plane direction and while it showed the opposite trend in the out-of-plane direction. These datasets and analyses represented a thorough study of the behavior of Nafion thin films on model substrates of interest, i.e., Pt catalyst/carbon electrodes. These results are expected to further understanding the difference in term of proton transport pathway.

1. Introduction

Development of energy generation, conversion, and storage technologies has been desired because the global demand for sustainable energy is rapidly increasing [1–4]. Among these new energy sources, polymer electrolyte fuel cells (PEFCs) are known for their high current density and use in portable energy solutions [5–8]. In typical polymer electrolyte fuel cells, the electrochemical reactions occur on the carbon-supported platinum (Pt/C) covered by a solid-state proton conducting electrolyte. Perfluorinated sulfonic acid ionomer (Nafion) is one of the most widely used proton-conducting materials owing to its high proton conductivity and thermal and chemical stability [9–11]. On the Pt/C catalyst, Nafion forms a semi-continuous film with nanoscale thickness, through which the transport of protons, water, and oxygen takes place [12–16]. Controlling the structure of the Nafion thin film on the Pt/C catalyst is important as the mass transport properties depend on it.

Nafion is composed of a hydrophobic polytetrafluoroethylene backbone (-CF_2-) with perfluorinated ether side-chains terminated by hydrophilic sulfonic acid groups (-SO_3H). The sulfonic acid groups exhibit high proton conductivity in a hydrophilic ionic domain [14,17–19]. Free-standing Nafion membranes, which are few hundred micrometers thick, have been widely investigated in the past decades [20–22]. Several studies have used cluster-network or the parallel water channel model to describe the nanostructure in the Nafion membranes. These membranes exhibit proton conductivity ranging from $\sim 10^{-1}$ to $\sim 10^{2}$ mS/cm under 10–100% relative humidity at 25 °C [14,23].

However, Nafion thin films on the Pt/C catalyst have a structure different from that of the free-standing Nafion membrane because of a strong confinement interaction between the thin film and the catalyst [24–28]. The proton conductivity of the Nafion thin films is one to two orders of magnitude lower than that of a free-standing Nafion membrane and shows strong thickness-dependence under a certain relative

* Corresponding author.
E-mail address: yamamoto.kentaro.4e@kyoto-u.ac.jp (K. Yamamoto).

https://doi.org/10.1016/j.ssi.2020.115456
Received 15 June 2020; Received in revised form 11 August 2020; Accepted 10 September 2020
Available online 24 September 2020

humidity [13,18]. The confinement effect is known to influence the phase behavior of uncharged block-copolymer systems [29–33]. In case of the thin films, as the thickness approach to the characteristic domain size of the block copolymers, the ionomer/substrate interactions can cause anisotropy in the orientation of the domains, resulting in that the morphology of the Nafion thin film differs from that of the free-standing Nafion membrane [30,34,35].

Grazing-incidence small-angle X-ray scattering (GISAXS) / grazing-incidence wide-angle X-ray scattering (GIWAXS) is a powerful tool to analyze the morphology of Nafion thin films [14,36–38]. GISAXS profiles of Nafion thin films, with thickness of 32–270 nm, cast on Pt, Au or carbon substrate, showed a scattering peak that was attributed to the hydrophilic domains [29]. The Nafion thin film on metallic substrate showed the sharpest scattering peak. In contrast, thin films on carbon substrate exhibited more isotropic behavior than the films on Au and Pt substrates. In the Si supported Nafion thin films with thickness of 25–100 nm was explored which showed that the thinner films show the lower degree of phase separation [30]. These results suggest that film thickness and substrate-ionomer interactions control the reorganization and alignment of the phase-separated nanostructure, thereby altering the water-transport and swelling properties [14,29,30,39–41].

Although many studies have focused on understanding the morphology or proton conductivity of the Nafion thin films, the quantitative relationship between morphology and proton conductivity of the Nafion thin films on Pt and/or carbon substrates has not been clarified. Especially, the proton conductivity of carbon supported Nafion thin films is still not explored. Our group previously reported the relationship between proton conductivity and morphology of Nafion thin films on Pt substrate with various thicknesses after annealing treatment via electrochemical impedance spectroscopy (EIS) and GISAXS/GIWAXS method [38]. In the process, we have developed the measurement method of proton conductivity of Nafion thin films on various substrate using self-designed interdigitated array electrodes.

The present study systematically analyzes the relationship between proton transport properties and morphology relationship of Pt and amorphous carbon supported cast thin films with thicknesses of 50–200 nm. Furthermore, the difference between Pt and carbon supported Nafion thin films in confinement effect / anisotropic behavior was discussed. The film thickness of Nafion thin films used in this study are thicker than the actual film thickness on membrane electrolyte assembly (MEA) with thickness of 2–5 nm [11,19], and the crystallinity of the carbon substrate is also different from the actual carbon support, such as Vulcan [2,3,33]. However, we believe that this paper will provide useful knowledge as a model of clarifying the actual proton transport in MEA.

2. Experimental

2.1. Sample preparations

5 wt% Nafion solution (Aldrich, EW = 1100) was diluted to desired concentration 0.1–1.6 wt% with 99.5% 1,1,1,3,3,3-hexafluoro-2-propanol (Wako Pure Chemical Industries, Ltd.).

The detailed information of pre-treatment of self-designed interdigitated array electrodes (Fig. S1) were described in our previous work [38]. Interdigitated array electrodes over carbon substrates were fabricated using the same method. The carbon substrate of was characterized by Raman microscope shown in Fig. S2. The carbon layer used in this study exhibited amorphous-like structure. As-prepared Nafion dispersion was dripped onto interdigitated array electrodes rotating at 800–1600 rpm for 2 min via the spin-cast method. The thickness of as-cast thin films were characterized by ellipsometry with Cauchy model fitting as we previously reported [38]. For GISAXS/GIWAXS measurements, Pt and carbon were deposited on Si substrate (1 cm × 1 cm). The thickness of as-prepared Nafion thin films was measured by ellipsometry. The ellipsometry mapping results were shown in Fig. S3. The difference in film thickness on a 2 mm square substrate was 0.2 nm or less when the Nafion film thickness is 10 nm and 6.2 nm or less when the Nafion thin films was 200 nm, which suggest that all samples used in this study are uniform.

2.2. Proton conductivity

The proton conductivity of the Nafion thin-films applied to the interdigitated array electrodes was measured using EIS under a flow of dry N_2 gas through water tank. All measurements were conducted at 25 °C with 20–90% relative humidity (RH). The impedance spectra were collected by applied an alternating potential of amplitude 100 mV with the frequency from 7 MHz to 0.01 Hz.

2.3. GISAXS/GIWAXS

GISAXS and GIWAXS were performed in beamline BL40B2 of SPring-8 in Hyogo, Japan. The wavelength was set as 0.1 nm. The experimental setup was shown in Fig. S4. GISAXS/GIWAXS measurements were conducted with 80% RH and at 25 °C. The GISAXS and GIWAXS 2D patterns were acquired with Pilatus imaging plate (0.172 mm × 0.172 mm pixel size, C9729DK-10) and flat panel sensor (0.05 mm × 0.05 mm, Hamamatsu Photonics K. K., Japan). The sample-to-detector distance was set at 2200 mm and 60 mm for GISAXS and GIWAXS, respectively. GISAXS and GIWAXS were measured at an incidence angle 0.14° and the exposure time was 100 s for all samples. The sample-to-detector distances were calibrated using a silver behenate and a cerium oxide for the GISAXS and GIWAXS measurements, respectively.

3. Results and discussion

Fig. 1 shows the proton conductivity of Nafion thin films cast on Pt and carbon substrates at 25 °C and various RH values. The collected Nyquist plot are shown in Fig. S5 in the supporting information. Both Pt- and carbon-supported Nafion thin films exhibit thickness dependence. Compared to the carbon-supported films, the Pt-supported films showed higher conductivity values at the same RH. In the case of 10-nm-thick films, proton conductivity of the Pt-supported specimen was more than an order of magnitude higher than that of the carbon-supported specimen. However, as the thickness approached 200 nm, the difference in proton conductivity of Pt and carbon-supported films reduced by an order of magnitude. This trend indicates that the bulk structure of the ionomer has more influence on the conductivity than its interaction with the substrate, as the thickness increases. Karan and Nagao's groups reported that the conductivity of Nafion thin film on SiO_2 showed similar tendencies and values [13,18]. Thus, it is considered that the results in Fig. 1 correctly reflect the actual differences in conductivity on these different substrates.

GISAXS measurements were performed to examine the morphological change of Nafion thin films relative to their thickness. Comparisons of GISAXS 2D patterns of Nafion thin films on Pt and carbon substrates

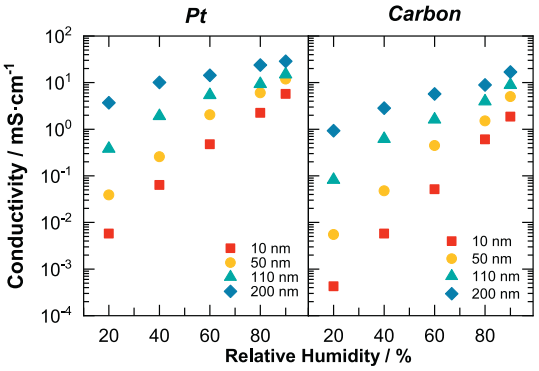

Fig. 1. Proton conductivity of Nafion thin films on Pt and carbon substrates with a variety of thicknesses and relative humidity at 25 °C.

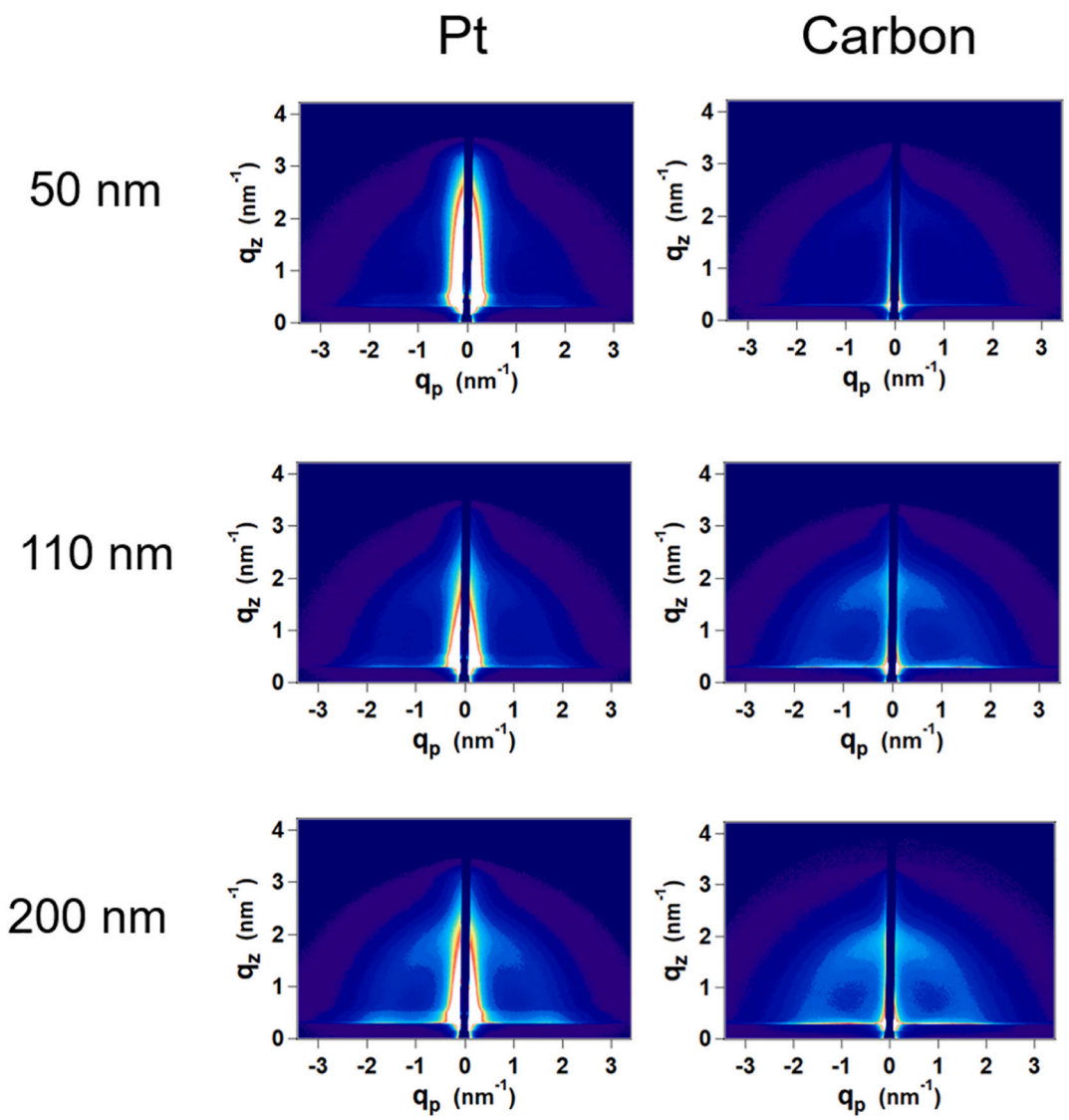

Fig. 2. GISAXS 2D patterns of Nafion thin films with a variety of thicknesses (50–200 nm) and substrate (Pt, carbon) measured at 80% RH and 25 °C.

are shown in Fig. 2. The scattering patterns are plotted in two dimensions as a function of the scattering vector q, which is defined in Eq. (1).

$$\mathbf{q} = \begin{pmatrix} q_x \\ q_y \\ q_z \end{pmatrix} = \frac{2\pi}{\lambda} \begin{pmatrix} \cos 2\Theta \cos \alpha_f - \cos \alpha_i \\ \sin 2\Theta \cos \alpha_f \\ \sin \alpha_i + \cos \alpha_f \end{pmatrix} \quad (1)$$

Here, λ represents the wavelength of the incident X-rays. The thickest film exhibited a scattering ring at q ~ 1.5–2 nm^{-1}, which is assigned to the ordered structure of the hydrophilic domains in Nafion thin film, and is called the "ionomer peak" [30]. Examination of the Pt- and carbon-supported samples at high humidity (Fig. 2) demonstrates that increasing thickness seems to cause more significant changes in films on Pt substrates than in films on carbon substrates. Similar with previous work, it is almost impossible to observe scattering ring in case of 10 nm-thick thin films under 80%RH at 25 °C as we shown in Fig. S6 due to the significant low intensity of ionomer peak or amorphous/crystalline peak [38].

To explore the variation of ionomer peaks in relation to the film thickness, line integral analysis was utilized to extract the I-q line profile. The cut lines along the equatorial and meridional direction reflect the ordered structure in-plane and out-of-plane, respectively. The as-obtained line-profiles of the Nafion thin films on Pt and carbon are shown in Fig. 3. It was found that the ionomer peak on Pt had a better-defined and sharper ionomer peak than carbon along the in-plane direction (a and b), suggesting a better-defined order in the ionic domain. However, when the film thickness decrease, the ionomer scattering peaks were not obvious, which indicate the existence of a less-ordered domain structure due to the strong confinement effect. Similar tendencies were found in the out-of-plane direction (Fig. 3c and d) as well.

Proton conductivity is a strong function of the humidity level and the proximity of adjacent ionic clusters. The former can be related to the relative humidity, and the latter can be interpreted as d-spacing. The latter is also a precursor and indicator of the ease of forming an H-bond network. Such a network is critical, especially with low relative humidity [42]. The ionomer peak observed in Fig. 3 was fitted to a Gaussian function, and the peak position values along the in-plane and out-of-plane directions were estimated (Fig. 3(a)). The scattering vector q, expressed in reciprocal space, was converted to d-spacing in real space using the following equation:

$$d = \frac{2\pi}{q} \quad (2)$$

As shown in Fig. 4(a), the ionomer peak shifted to higher d-spacing values with increasing film thickness in both samples owing to the growth of the ionic domains. Along the in-plane direction, the d-spacing of the ionic domains in Pt- and carbon supported films increased from 3.9 to 4.6 nm and from 3.5 to 3.7 nm, respectively.

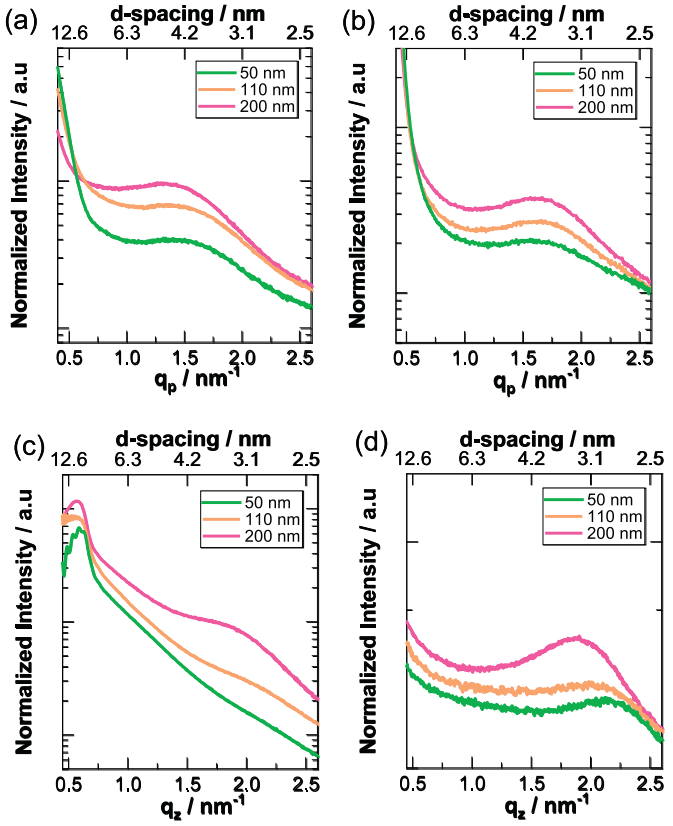

Fig. 3. GISAXS 1D line-profile along the in-plane: (a) Pt and (b) Carbon, and out-of-plane: (c) Pt and (d) Carbon.

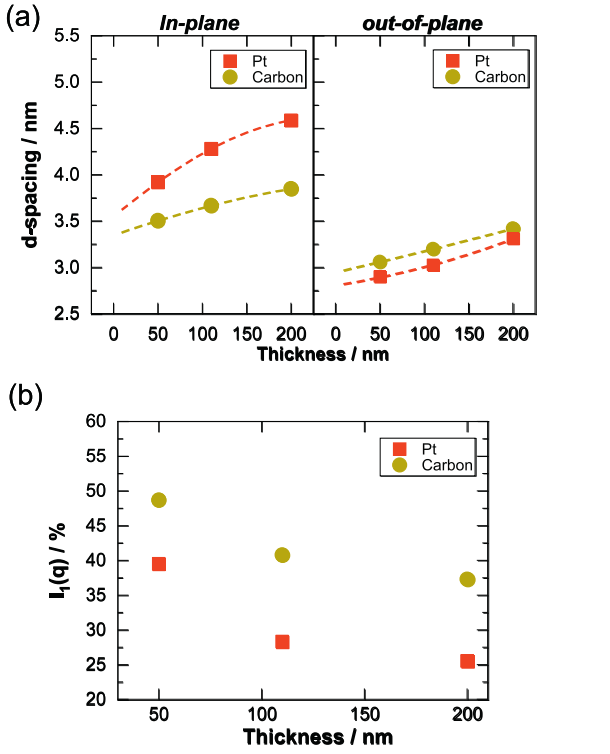

Fig. 4. (a) d-spacing of hydrophilic ionic domain extracted from Fig. 3 in-plane and out-of-plane with 80% RH at 25 °C. (b) Ratio of the ionomer contribution along the out-of-plane direction. The values were calculated on the basis of $I_1(q) / (I_1(q) + I_2(q)) \times 100$.

Periodic ionic domains and semi-crystalline hydrophobic structures were formed in the 50-nm-thick films, which led to higher conductivity values. For the Nafion thin films with thickness over 110 nm, the hydrophilic domains grew considerably because of the relatively stronger nanophase separation than that in the thinner films. The hydrophilic domains, which act as the protonic path, grew larger with increasing humidity and thickness, leading to a lower activation energy of the proton conduction process.

In order to quantitatively comparison of the intensity of ionomer peak along meridional and equatorial axes, represented as I_1 and I_2, respectively, we normalized the curves using the integrated intensity of ionomer peak with same method as our previous work [38]. I_1 (out-of-plane) and I_2 (in-plane) are assumed to be Gaussian distribution functions of the azimuthal angle φ, with peaks along the meridional (φ = 0°) and equatorial (φ = 90°) direction, respectively. The obtained I_1 (φ) and I_2 (φ) were then used to determine the normalized intensity I (q), as defined by the following equation [43].

$$I_i(q) \approx \int_0^{\frac{\pi}{2}} I_i(\varphi) 2\pi q \ |\sin\varphi| \ d\varphi \tag{3}$$

The normalized intensity of the ionomer peak along the meridian (i = 1) and the equator (i = 2) was evaluated using Eq. (3). An illustration of a typical azimuthal plot fitting is shown in Fig. S7. For all samples, a low χ^2 value (≤ 2.19) was obtained.

As shown in Fig. 4(b), the $I_1(q)$ (%) increased with decreasing thickness, regardless of substrate, which indicate that the contribution of out-of-plane component comparatively increased as decreasing thickness. Additionally, the $I_1(q)$ on the Pt was comparatively lower than that on the carbon, which suggest that the hydrophilic domain in Pt-supported Nafion is more orientated. Furthermore, it might indicate the hydrophilic domains grew better along the in-plane direction on Pt than on carbon. The hydrophilic domains in Nafion thin films show different anisotropic behavior depending on the substrate. The substrate influences the crystalline phase of the fluorocarbon backbone as well as the hydrophilic ionic domains in the Nafion films. To examine the molecular aggregation in the hydrophobic domains of the Nafion films, GIWAXS measurements were performed at 25 °C and 80% RH. Fig. S8 shows the 2D GIWAXS patterns and Fig. 5 shows the GIWAXS line profiles of the Nafion thin films on Pt and carbon substrates.

The influence of the substrate was evident from variation of a scattering halo indicative of amorphous/crystalline component. For instance, the line profiles (Fig. 5(a)) showed that increasing thickness caused a crystalline peak to appear near q = 11 nm^{-1}, which was next to the amorphous peak at 9.5 nm^{-1} [29,44,45]. This thickness-induced crystalline order, with a characteristic spacing around 0.5 nm, corresponds to the (-CF_2-) backbone chains of the polytetrafluoroethylene crystallites, similar to the typical wide angle X-ray scattering peak observed for the free-standing Nafion membranes [29]. These crystallites form a crystalline structure, which leads to physical crosslinking of the (-CF_2-) backbone and consequent reduction in the proton conductivity. The formation of a crystalline order was observed in Fig. 5 by the shifts in the crystalline peak around q = 11 nm^{-1}. For both Pt- and carbon-supported thin films, as the film thickness decreased to 50 nm, (Fig. 5(a) and (b)), the crystalline order is expected to decrease, because the backbone chains become topologically confined at such a thickness [33]. Additionally, in case of Pt-supported Nafion thin films, it is notable that the observed amrophous/crystalline peak in out-of-plane component is more defined and sharper than that of in-plane component. The opposite phenomenon was observed for carbon-supported thin films.

Here, we introduced an indicator: crystalline-rich domain proportion (P_c-rich), to gain further insight regarding the relative variation in the semi-crystalline (-CF_2-) backbone aggregation on different substrates. Fig. 6 shows the P_c-rich in various Nafion thin films; the P_c-rich values were extracted from the as-obtained 2D scattering parttern (Fig. S8). The detail of the calculation method is described in Fig. S9 and our previous study [38]. Generally, the P_c showed thickness dependence on both substrates. Interestingly, P_c-rich of the thin films on the Pt

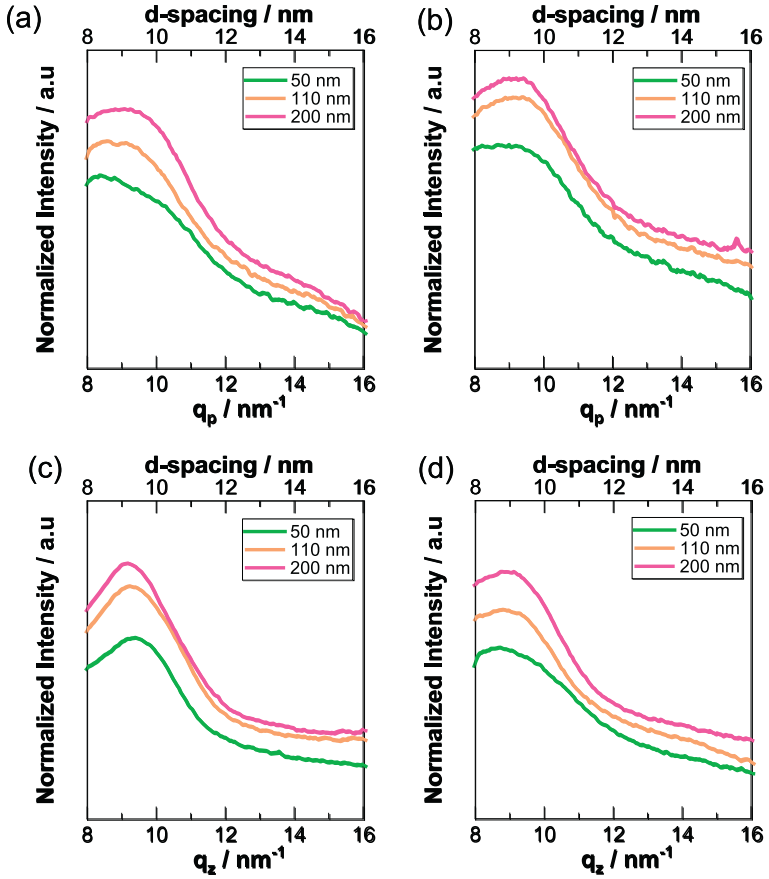

Fig. 5. GIWAXS line-profile extracted from 2D patterns of Nafion thin films in-plane: (a) Pt and (b) Carbon, and out-of-plane: (c) Pt and (d) Carbon.

substrate along the out-of-plane direction showed higher values than that on the carbon substrate, while showing the opposite trend along the in-plane direction.

We have shown our conceptual model of the morphology of Nafion thin films with thickness ranging from 50 to 200 nm on Pt and carbon substrates in Fig. 7. In the case of the Nafion thin film with 50 nm thickness, the hydrophilic domain along in-plane direction in Pt-supported Nafion thin films is comparatively larger than carbon supported Nafion thin films. This is because the interaction between the sulfonic acid and Pt is relatively strong than the interaction between the sulfonic acid and carbon [29]. The development of hydrophilic domain on Pt substrate increase the proton conductivity, compared to carbon substrate as shown in Fig. 1. The in-plane proton conductivity difference between Pt and carbon becomes small as the thickness of Nafion thin-film increases because the interaction between ionomer and substrate becomes relatively small. On the other hand, we proved that the hydrophilic domain along in-out-of-plane direction in Pt-supported Nafion thin films is comparatively smaller than carbon supported Nafion thin films. It is anticipated that the proton conductivity along out-of-plane direction of Pt supported Nafion thin films is not be as high as carbon supported thin films based on the relationship between the hydrophilic domain and proton conductivity of in-plane in Nafion thin films. For more quantitative comparison, it is necessary to consider the effect of the connectivity of hydrophilic domains and size of crystalline-phase in the Nafion thin films.

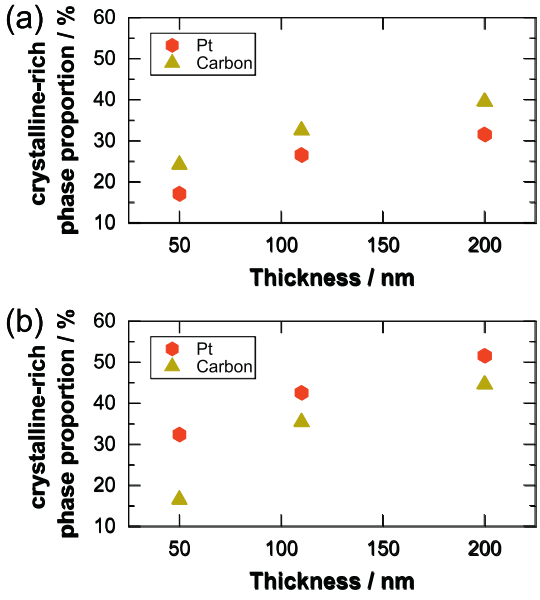

Fig. 6. The Crystalline-rich phase proportion in Nafion thin films of various thicknesses and on different substrates along (a) In-plane and (b) Out-of-plane directions.

4. Conclusion

We focused on a series of Nafion films with thickness ranging from 50 to 200 nm to reveal differences in confinement effect and impacts from type of substrate. This was done in terms of morphology and proton transport property via GISAXS/GIWAXS and the electrochemical impedance method. Within this range of film thickness, substrate/ionomer interaction are expected to have a significant impact on the structure of the ionomer. Thin films on Pt exhibit completely different anisotropic behavior than those on carbon substrate. In the case of Pt, that the hydrophilic ionic domain along the in-plane direction is more developed than that along the out-of-plane shows significant

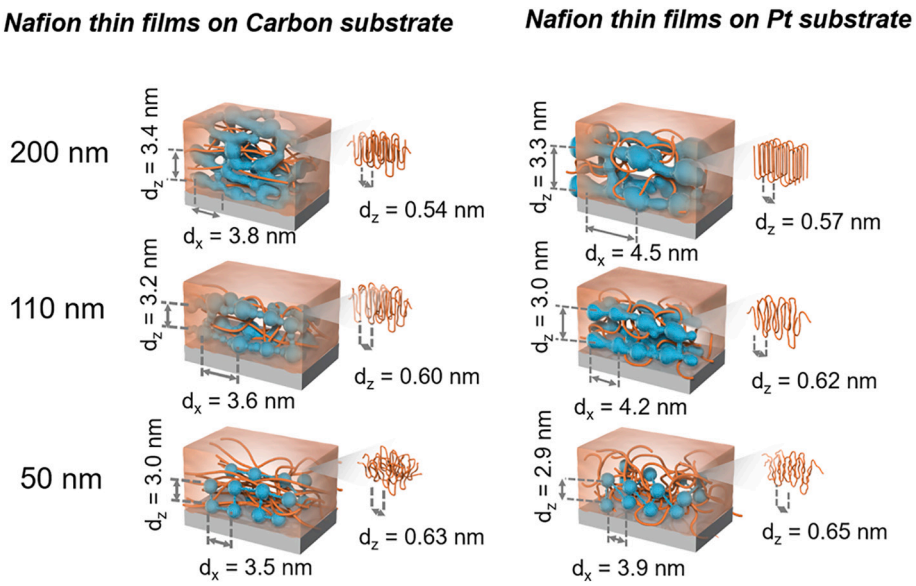

Fig. 7. Schematic image of Nafion thin film structure with different morphological behavior on carbon and Pt substrates.

anisotropic behavior. Interestingly, as the film thickness reaches, in essence, bulk phase (200 nm), the difference in conductivity between carbon and Pt substrates becomes almost negligible. It is anticipated that the proton in-plane conductivity in the Nafion thin films is higher than out-of-plane conductivity, because the in-plane size of the hydrophilic domains is larger than their out-of-plane size. The knowledge about the relationship between the proton transport and morphology of Pt and carbon supported Nafion thin films, is useful to design proton transport pathway of practical catalyst.

Declaration of Competing Interest

The authors declare that they have no known competing financial interests or personal relationships that could have appeared to influence the work reported in this paper.

Acknowledgement

This research is based on results obtained from a project commissioned by the New Energy and Industrial Technology Development Organization (NEDO). This study was partially supported by the Synchrotron radiation experiments performed at BL40B2 of SPring-8 with the approval of the Japan Synchrotron Radiation Research Institute (JASRI) (Proposal Nos. 2016B1013, 2017A1020, 2017B1044, 2018A1020, 2018B1034, 2019A1025, 2019B1023, 2019B1024).

Appendix A. Supplementary data

Supplementary data to this article can be found online at https://doi.org/10.1016/j.ssi.2020.115456.

References

[1] M. Eikerling, A. Kulikovsky, Polymer Electrolyte Fuel Cells: Physical Principles of Materials and Operation, CRC Press, 2014.
[2] A.A. Franco, Polymer Electrolyte Fuel Cells: Science, Applications, and Challenges, Pan Stanford Publishing, 2016.
[3] K.D. Kreuer, Fuel Cells: Selected Entries from the Encyclopedia of Sustainability Science and Technology, Springer, New York, 2012.
[4] H. Li, S. Knights, Z. Shi, J.W. Van Zee, J. Zhang, Proton Exchange Membrane Fuel Cells: Contamination and Mitigation Strategies, CRC Press, 2010.
[5] R. O'Hayre, S.W. Cha, F.B. Prinz, W. Colella, Fuel Cell Fundamentals, Wiley, 2016.
[6] H. Pu, Polymers for PEM Fuel Cells, Wiley, 2014.
[7] E. Santos, W. Schmickler, Catalysis in Electrochemistry: From Fundamental Aspects to Strategies for Fuel Cell Development, Wiley, 2011.
[8] J. Zhang, J. Wu, H. Zhang, PEM Fuel Cell Testing and Diagnosis, Elsevier Science, 2013.
[9] K.A. Mauritz, R.B. Moore, State of understanding of Nafion, Chem. Rev. 104 (2004) 4535–4586.
[10] W. Sheng, S. Chen, E. Vescovo, Y. Shao-Horn, Size influence on the oxygen reduction reaction activity and instability of supported Pt nanoparticles, J. Electrochem. Soc. 159 (2012) B96–B103.
[11] S. Holdcroft, Fuel cell catalyst layers: a polymer science perspective, Chem. Mater. 26 (2014) 381–393.
[12] R. Jinnouchi, K. Kudo, N. Kitano, Y. Morimoto, Molecular dynamics simulations on O_2 permeation through Nafion Ionomer on platinum surface, Electrochim. Acta 188 (2016) 767–776.
[13] D.K. Paul, R. McCreery, K. Karan, Proton transport property in supported Nafion Nanothin films by electrochemical impedance spectroscopy, J. Electrochem. Soc. 161 (2014) F1395–F1402.
[14] M.A. Modestino, D.K. Paul, S. Dishari, S.A. Petrina, F.I. Allen, M.A. Hickner, K. Karan, R.A. Segalman, A.Z. Weber, Self-assembly and transport limitations in confined Nafion films, Macromolecules 46 (2013) 867–873.
[15] Z. Siroma, T. Ioroi, N. Fujiwara, K. Yasuda, Proton conductivity along interface in thin cast film of Nafion®, Electrochem. Commun. 4 (2002) 143–145.
[16] Z. Siroma, R. Kakitsubo, N. Fujiwara, T. Ioroi, S.-i. Yamazaki, K. Yasuda, Depression of proton conductivity in recast Nafion® film measured on flat substrate, J. Power Sources 189 (2009) 994–998.
[17] K. Schmidt-Rohr, Q. Chen, Parallel cylindrical water nanochannels in Nafion fuel-cell membranes, Nat. Mater. 7 (2008) 75–83.
[18] Y. Ono, Y. Nagao, Interfacial structure and proton conductivity of Nafion at the Pt-deposited surface, Langmuir 32 (2016) 352–358.
[19] A. Kusoglu, A.Z. Weber, New insights into Perfluorinated sulfonic-acid ionomers, Chem. Rev. 117 (2017) 987–1104.
[20] K.-D. Kreuer, S.J. Paddison, E. Spohr, M. Schuster, Transport in proton conductors for fuel-cell applications: simulations, elementary reactions, and phenomenology, Chem. Rev. 104 (2004) 4637–4678.
[21] K.-D. Kreuer, G. Portale, A critical revision of the Nano-morphology of proton conducting Ionomers and polyelectrolytes for fuel cell applications, Adv. Funct. Mater. 23 (2013) 5390–5397.
[22] Q. Berrod, S. Lyonnard, A. Guillermo, J. Ollivier, B. Frick, A. Manseri, B. Améduri, G. Gébel, Nanostructure and transport properties of proton conducting self-assembled Perfluorinated surfactants: a bottom-up approach toward PFSA fuel cell membranes, Macromolecules 48 (2015) 6166–6176.
[23] M.P. Rodgers, L.J. Bonville, H.R. Kunz, D.K. Slattery, J.M. Fenton, Fuel cell perfluorinated sulfonic acid membrane degradation correlating accelerated stress testing and lifetime, Chem. Rev. 112 (2012) 6075–6103.
[24] D.K. Paul, A. Fraser, K. Karan, Towards the understanding of proton conduction mechanism in PEMFC catalyst layer: conductivity of adsorbed Nafion films, Electrochem. Commun. 13 (2011) 774–777.
[25] D.K. Paul, K. Karan, Conductivity and wettability changes of ultrathin Nafion films subjected to thermal annealing and liquid water exposure, J. Phys. Chem. C 118 (2014) 1828–1835.
[26] B.R. Frieberg, K.A. Page, J.R. Graybill, M.L. Walker, C.M. Stafford, G.R. Stafford, C.L. Soles, Mechanical response of thermally annealed Nafion thin films, ACS Appl. Mater. Interfaces 8 (2016) 33240–33249.
[27] Y. Nagao, Highly oriented sulfonic acid groups in a Nafion thin film on Si substrate, J. Phys. Chem. C 117 (2013) 3294–3297.
[28] S.K. Dishari, M.A. Hickner, Confinement and proton transfer in NAFION thin films,

Macromolecules 46 (2013) 413–421.
[29] A. Kusoglu, D. Kushner, D.K. Paul, K. Karan, M.A. Hickner, A.Z. Weber, Impact of substrate and processing on confinement of Nafion thin films, Adv. Funct. Mater. 24 (2014) 4763–4774.
[30] A. Kusoglu, T.J. Dursch, A.Z. Weber, Nanostructure/swelling relationships of bulk and thin-film PFSA Ionomers, Adv. Funct. Mater. 26 (2016) 4961–4975.
[31] M. Plazanet, R. Torre, F. Sacchetti, Confinement, entropic effects and hydrogen bond network fluctuations of water in Nafion membrane, J. Mol. Liq. 219 (2016) 1161–1164.
[32] M. Tesfaye, A.N. MacDonald, P.J. Dudenas, A. Kusoglu, A.Z. Weber, Exploring substrate/ionomer interaction under oxidizing and reducing environments, Electrochem. Commun. 87 (2018) 86–90.
[33] K. Karan, Interesting facets of surface, interfacial, and bulk characteristics of Perfluorinated Ionomer films, Langmuir 35 (2019) 13489–13520.
[34] K.A. Page, A. Kusoglu, C.M. Stafford, S. Kim, R.J. Kline, A.Z. Weber, Confinement-driven increase in ionomer thin-film modulus, Nano Lett. 14 (2014) 2299–2304.
[35] M. Tesfaye, D.I. Kushner, A. Kusoglu, Interplay between swelling kinetics and nanostructure in Perfluorosulfonic acid thin-films: role of hygrothermal aging, ACS Appl. Polymer Mater. 1 (2019) 631–635.
[36] M. Bass, A. Berman, A. Singh, O. Konovalov, V. Freger, Surface structure of Nafion in vapor and liquid, J. Phys. Chem. B 114 (2010) 3784–3790.
[37] M. Bass, A. Berman, A. Singh, O. Konovalov, V. Freger, Surface-induced micelle orientation in Nafion films, Macromolecules 44 (2011) 2893–2899.
[38] X. Gao, K. Yamamoto, T. Hirai, T. Uchiyama, N. Ohta, N. Takao, M. Matsumoto, H. Imai, S. Sugawara, K. Shinohara, Morphology changes in Perfluorosulfonated Ionomer from thickness and thermal treatment conditions, Langmuir 36 (2020) 3871–3878.
[39] K. Karan, PEFC catalyst layer: recent advances in materials, microstructural characterization, and modeling, Abbrev: Curr. Opin. Electrochem 5 (2017) 27–35.
[40] D.I. Kushner, A. Kusoglu, N.J. Podraza, M.A. Hickner, Substrate-dependent molecular and Nanostructural orientation of Nafion thin films, Adv. Funct. Mater. 1902699 (2019).
[41] P.J. Goossens, B. Vallaey, J. Verlinden, J.A. Martens, J. Rongé, Interfacial water drives improved proton transport in siliceous Nanocomposite Nafion thin films, ChemPhysChem 19 (2018) 538–546.
[42] H. Iden, K. Sato, A. Ohma, K. Shinohara, Relationship among microstructure, Ionomer property and proton transport in Pseudo catalyst layers, J. Electrochem. Soc. 158 (2011) B987–B994.
[43] Y. Shoji, R. Ishige, T. Higashihara, J. Morikawa, T. Hashimoto, A. Takahara, J. Watanabe, M. Ueda, Cross-linked liquid crystalline polyimides with Siloxane units: their morphology and thermal diffusivity, Macromolecules 46 (2013) 747–755.
[44] P.C. van der Heijden, L. Rubatat, O. Diat, Orientation of drawn Nafion at molecular and Mesoscopic scales, Macromolecules 37 (2004) 5327–5336.
[45] G.A. Giffin, G.M. Haugen, S.J. Hamrock, V. Di Noto, Interplay between structure and relaxations in Perfluorosulfonic acid proton conducting membranes, J. Am. Chem. Soc. 135 (2013) 822–834.